()

Nondestructive depth-resolved spectroscopic investigation of the heavily intermixed $In_2S_3/Cu(In,Ga)Se_2$ interface

M. Bär,[1,2,)] N. Barreau,[3,)] F. Couzinié-Devy,[3] S. Pookpanratana,[2] J. Klaer,[1] M. Blum,[2,4] Y. Zhang,[2] W. Yang,[5] J. D. Denlinger,[5] H.-W. Schock,[1] L. Weinhardt,[4] J. Kessler,[3] and C. Heske[2,)]

[1]*Solar Energy Research, Helmholtz-Zentrum Berlin für Materialien und Energie GmbH, Lise-Meitner-Campus, Hahn-Meitner-Platz 1, 14109 Berlin, Germany*
[2]*Department of Chemistry, University of Nevada, Las Vegas (UNLV), Las Vegas, Nevada 89154-4003, USA*
[3]*Institut des Matériaux Jean Rouxel (IMN)-UMR 6502, Université de Nantes, CNRS, 2 rue de la Houssinière, BP 32229, 44322 Nantes Cedex 3, France*
[4]*Experimentelle Physik VII, Universität Würzburg, 97074 Würzburg, Germany*
[5]*Advanced Light Source (ALS), Lawrence Berkeley National Laboratory, Berkeley, California 94720, USA*

()

The chemical structure of the interface between a nominal In_2S_3 buffer and a $Cu(In,Ga)Se_2$ (CIGSe) thin-film solar cell absorber was investigated by soft x-ray photoelectron and emission spectroscopy. We find a heavily intermixed, complex interface structure, in which Cu diffuses into (and Na through) the buffer layer, while the CIGSe absorber surface/interface region is partially sulfurized. Based on our spectroscopic analysis, a comprehensive picture of the chemical interface structure is proposed. []

$Cu(In,Ga)Se_2$ (CIGSe) thin-film solar cells with an n^+-ZnO/i-ZnO/CdS/CIGSe/Mo/glass device structure have reached efficiencies of 20%.[1] To replace the CdS layer by a nontoxic, more transparent buffer, and the conventionally used chemical bath deposition by a technique allowing in-line processing, In_2S_3 layers have been deposited by physical vapor deposition,[2] sputtering,[3] atomic layer deposition,[4] and spray ion layer gas reaction.[5]

The In_2S_3/CIGSe interface has been previously investigated by different destructive depth-profiling techniques,[2,6] high-resolution transmission electron microscopy and energy dispersive x-ray analysis,[7] and x-ray photoelectron spectroscopy (XPS).[4,8,9] At (post-)deposition annealing temperatures necessary for high device efficiencies (200–250 °C), a pronounced diffusion of Cu and Na from the CIGSe/Mo/glass substrate into the *nominal* In_2S_3 buffer layer was found in these studies. However, a complete picture of the chemical interface structure is still missing. In this paper, we will report on the characterization of the In_2S_3/CIGSe interface by a combination of nondestructive techniques [XPS and soft x-ray emission spectroscopy (XES)], deliberately varying the probing depth. Our measurements result in a *depth-resolved* picture of the interface in unprecedented detail.

In_2S_3/CIGSe structures were prepared at IMN on Mo/glass substrates.[10] The absorber layers were dipped in NH_3 solution (1 M, room temperature, 1 min) prior to the In_2S_3 buffer layer deposition by thermal coevaporation of elemental indium and sulfur at 200 °C substrate temperature. To vary the In_2S_3 thickness, different deposition times were used. The standard 80 nm buffer used in solar cells is prepared in 10 min (called "1/1" in the following). For reference, an In_2S_3 layer, different In_2S_3:Cu standards, and a $CuInS_2$ (CIS) absorber[11] were deposited on Mo/glass substrates. After preparation, all samples were sealed in polyethylene bags filled with dry N_2 and desiccant for transport. At UNLV the samples were transferred into the analysis chamber (base pressure $<5\times10^{-10}$ mbar) without air exposure. XPS was performed using Mg K_α and Al K_α excitation and a Specs PHOIBOS 150 MCD electron analyzer (calibrated according to Ref. 12). Subsequently, XES was performed at the ALS using the soft x-ray fluorescence endstation of Beamline 8.0.

XPS survey spectra (not shown) show all expected absorber photoemission lines, Na-related peaks, and only minor spectral contributions of C- and O-containing surface contaminants. The former is due to the well-known diffusion of Na from the soda-lime glass substrate through the Mo and CIGSe layers,[13] the latter indicates an IMN-to-UNLV sample transfer with minimal sample contamination. Upon In_2S_3 deposition, S-related peaks can also be observed. Furthermore, the intensity of all absorber-related lines (except In) decreases. However, we find significant differences in the attenuation behavior of the different CIGSe-related peaks. We have thus quantified the corresponding photoemission lines by a simultaneous fit of the spectra of all samples, using Voigt profiles and a linear background. For spin-orbit doublets, the respective, Gaussian and Lorentzian widths were coupled for each component and for all samples, and the intensity ratio was fixed according to the $(2j+1)$ multiplicity. Figure 1(a) shows the intensity evolution of the different photoemission lines upon In_2S_3 deposition, normalized to the corresponding peak intensities of the bare (i.e., uncovered but NH_3-etched) CIGSe absorber and the 1/1-In_2S_3/CIGSe sample, respectively. As expected, the intensities of the S- and In-related lines increase, while those of the Ga- and Se-related peaks decrease. In accordance with the diffusion found in Refs. 4 and 7–9, the Cu signal only decreases to approximately 40% of its initial intensity. The Na 1*s* intensity first increases and then decreases again to the same level as for the bare CIGSe surface. While the attenuation of the Se- and Ga-related peaks indicates a complete coverage of the absorber, the significant intensities for the Cu and Na signals point to a heavily intermixed interface between the In_2S_3 buffer and the absorber, in agreement with earlier

)

( )

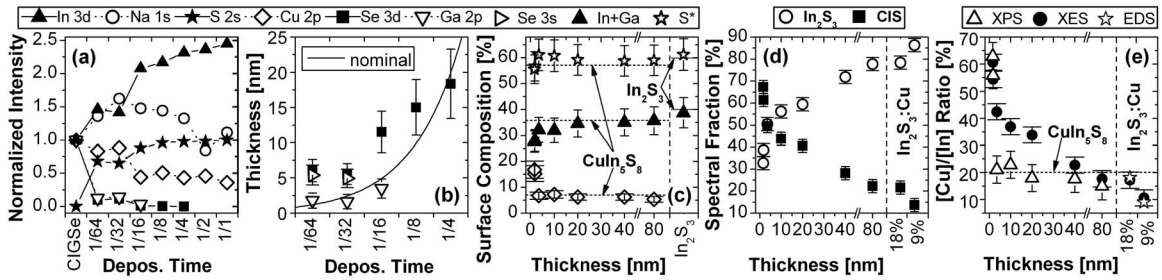

FIG. 1. (a) Evolution of the XPS line intensities with increasing In_2S_3 deposition time (error bars are in the range of symbol size). The latter is given as fraction of 10 min (the standard buffer deposition time). (b) Comparison of the nominal thickness of the In_2S_3 buffer with values calculated from the attenuation of different photoemission lines. (c) Surface composition of the investigated In_2S_3/CIGSe samples (as a function of buffer thickness) and of an In_2S_3 reference, as computed from the measured XPS data. For comparison, the stoichiometry of a $CuIn_5S_8$ and In_2S_3 is indicated. (d) Spectral fractions of CIS and In_2S_3 S $L_{2,3}$ XES reference spectra in the spectra of the buffer thickness series. The corresponding fractions in the S $L_{2,3}$ XES spectra of the In_2S_3:Cu standards (with nominal 9% and 18% Cu content) are shown for control. (e) Comparison of [Cu]/[In] ratios determined from XPS and XES. For the In_2S_3:Cu standard samples, the EDS ratio is shown as reference (instead of the XPS ratio). The [Cu]/[In] ratio of a $CuIn_5S_8$ compound is also indicated.

findings[8] (we will nevertheless continue to refer to the deposited layer as In_2S_3 in the following).

The fact that the Se 3*d* signal decreases similarly to the Ga 2*p* signal is surprising, since the inelastic mean free path[14] (λ) of the corresponding Se 3*d* photoelectrons (~2.5 nm in pure In_2S_3 using Mg K_α excitation) is significantly higher than that of the Ga 2*p* photoelectrons (~0.5 nm). We have computed the corresponding effective In_2S_3 thickness (*d*), assuming homogeneous and conformal absorber coverage, using $I = I_0 \times \exp(-d/\lambda)$, where I (I_0) is the (un)attenuated signal intensity. Figure 1(b) shows the different effective thicknesses based on the attenuation of the Ga- and Se-related peaks (average of the Mg and Al K_α XPS measurements) in comparison with the nominal thickness. We observe that the Ga 2*p*-based effective thickness is (within the error bars) in good agreement with the nominal thickness, while the Se 3*d*- and Se 3*s*-based effective thicknesses are significantly increased. Only for the thickest overlayer sample with observable Se signal (the 1/4 sample) do we observe an agreement with the nominal thickness. This finding could be due to a partial substitution of Se by S at the absorber surface, combined with a subsequent selenium sublimation (favored by the high selenium vapor pressure) in the first stages of In_2S_3 deposition. Although Se depletion of CIGSe surfaces due to vacuum annealing has not been reported for temperatures below 600 °C,[15] temperatures in the range of the used substrate temperature for our In_2S_3 deposition are applied to re-evaporate Se caps from CIGSe.[16] Furthermore, similar S/Se substitution processes have been observed upon CIGSe exposure to H_2S atmosphere at high temperatures[17] and after low-temperature chemical bath deposition of CdS.[18]

Note that the calculated layer thicknesses for the 1/64- and 1/32-In_2S_3/CIGSe samples are—within the error bars—identical. Hence, we are using the computed thickness for thin In_2S_3 (instead of the nominal buffer thickness) as the comparative parameter for the following considerations.

To quantify the XPS data, the respective peak intensities were first corrected by the corresponding λ (Ref. 14) and photoionization cross section,[19] as well as by the electron analyzer transmission. We find that both the Cu/Na and In/Na [S/Na] ratios measured with Al K_α are $(47 \pm 2)\%[(16 \pm 1)\%]$ higher than those in the more surface-sensitive Mg K_α experiments. Our findings thus point to an accumulation of Na at all sample surfaces. The smaller Al K_α/Mg K_α difference for the S/Na ratio might indicate that also comparatively more S is present at the sample surface. We tentatively explain this with a formation of S–Na bonds at the In_2S_3/CIGSe sample surface. However, the presence of Na in the buffer bulk can also not be excluded.

The surface composition based on the XPS signal intensities is shown in Fig. 1(c) as a function of In_2S_3 thickness. Note that the S content was corrected to account for a possible Na_2S formation at the surface: $S^* = [S] - 1/2 \times [Na]$. For In_2S_3 thicknesses above 5 nm, the Cu:In:S composition is constant and in good agreement with a 1:5:8 stoichiometry, as indicated. This suggests a homogeneous buffer layer composition, independent of buffer layer thickness. For verification purposes, the determined In:S composition ([39:61]%) of an In_2S_3 reference layer is also shown.

To enhance bulk-sensitivity, we additionally characterized the In_2S_3/CIGSe samples with the more bulk-sensitive XES. Selected S $L_{2,3}$ XES spectra are shown in Fig. 2(a). The spectrum of the bare (S-free) CIGSe absorber is ascribed to the significantly less intense Se $M_{2,3}$ emission (note the magnification factor of ×10). In contrast, the S $L_{2,3}$ emission dominates the spectra even for the thinnest In_2S_3 layer. Apart from the expected increase in intensity with In_2S_3

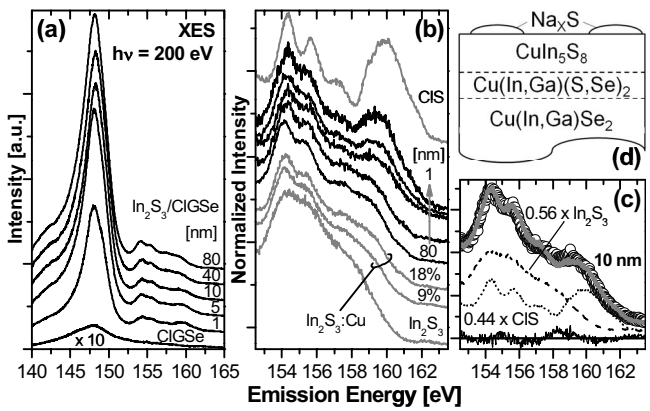

FIG. 2. (a) S $L_{2,3}$ XES spectra of the In_2S_3/CIGSe samples. (b) Magnified valence band region, together with a CIS and In_2S_3 reference and In_2S_3:Cu standards (with nominal Cu contents of 9% and 18%, respectively). (c) S $L_{2,3}$ XES valence band region of the 10 nm In_2S_3/CIGSe sample (open circles: raw data; gray line: fit) as superposition of In_2S_3 and CIS contributions. The residuum (i.e., the difference between raw data and fit) is shown at the bottom. (d) Simplified scheme of the proposed chemical structure of the surface region of a standard In_2S_3/CIGSe sample.

thickness, the S $L_{2,3}$ spectra of all In_2S_3/CIGSe samples look very similar at first glance. A closer look at the valence band features[20] between 153 and 163 eV in Fig. 2(b), however, reveals significant differences between the samples. The comparison with corresponding reference spectra shows that the S $L_{2,3}$ spectra for thin In_2S_3 layers are similar to that of the CIS reference, while the S $L_{2,3}$ spectrum of the thick In_2S_3/CIGSe samples resembles that of the In_2S_3:Cu standards quite well.

To quantify the XES data, we used a sum of the CIS and In_2S_3 reference spectra to (least-square) fit the valence band region, as exemplarily shown for the 10 nm In_2S_3/CIGSe sample in Fig. 2(c). The resulting spectral CIS and In_2S_3 fractions are shown in Fig. 1(d). The CIS fraction is decreasing and the In_2S_3 fraction is increasing with In_2S_3 layer thickness. The quantified values confirm that the thick In_2S_3/CIGSe sample is very similar to the In_2S_3:Cu(18%) standard.

Assuming that the reference spectra represent stoichiometric CIS and In_2S_3 samples and that the S $L_{2,3}$ spectra of the In_2S_3/CIGSe samples can exclusively be represented as the superposition of the reference spectra, we compute a [Cu]/[In] ratio from the CIS and In_2S_3 fractions: $[Cu]/[In]=1/2\times S\,L_{2,3}(CIS)/[1/2\times S\,L_{2,3}(CIS)+2/3\times S\,L_{2,3}(In_2S_3)]$. This ratio, which by design only takes into account Cu and In atoms *bound to S*, is shown in Fig. 1(e), together with the XPS-derived (total) [Cu]/[In] ratio. For the In_2S_3:Cu standards, the [Cu]/[In] ratios measured by energy dispersive x-ray spectroscopy[21] (EDS) are also shown and agree very well with the XES-based ratios. For the In_2S_3/CIGSe samples, we find similar XPS and XES [Cu]/[In] ratios for the thinnest and thickest but not the intermediate In_2S_3 layers. The expected similar values for the thick samples are in agreement with a homogeneous $CuIn_5S_8$ composition throughout the entire buffer. Since S $L_{2,3}$ XES spectra only probe the chemical environment of the S atoms, only the S-containing $CuIn_5S_8$ compound [formed on a S-free (!) CIGSe] contributes to the respective spectra. Assuming a homogeneous $CuIn_5S_8$ composition (i.e., no Cu gradient), the XES [Cu]/[In] ratio of all In_2S_3/CIGSe samples should thus be similar to that of the formed $CuIn_5S_8$ buffer compound. The observed deviation for low thicknesses is ascribed to the substitution of Se by S in the CIGSe surface/interface region during the first stages of the In_2S_3 deposition, probably forming a $Cu(In,Ga)(S,Se)_2$ interlayer. The difference between the XPS and XES [Cu]/[In] ratios for the intermediate In_2S_3 thicknesses is due to the different information depths of the techniques (more precisely: by λ of electrons and by the much larger attenuation length of photons [here approx. 30 nm]).[22] In the early stages of the In_2S_3 deposition, the buffer is thin enough such that the (sulfurized) CIGSe side of the In_2S_3/CIGSe interface gives a significant contribution to both XPS and XES spectra, leading to high [Cu]/[In] ratios. Then, with increasing thickness, the contribution of the In_2S_3/CIGSe interface region is reduced, in particular for XPS ($\lambda_{Cu\ 2p}\sim 1$ nm). As a result, the XPS-derived ratio rapidly decreases to the $CuIn_5S_8$ level. Due to the larger information depth the XES spectra, in contrast, still contain a substantial contribution from the interface region. This results in a much slower decrease in the [Cu]/[In] ratio.

The scheme in Fig. 2(d) summarizes the findings of our XPS and XES investigation. We suggest that, during In_2S_3 coevaporation on a CIGSe substrate, a $CuIn_5S_8$ buffer is formed, the absorber surface/interface region is chemically modified by a partial substitution of Se by S [probably resulting in a $Cu(In,Ga)(S,Se)_2$ interlayer], and Na and S accumulate at the sample surface, possibly forming Na_xS islands or a thin film. Acting as a Cu source for the $CuIn_5S_8$ formation, the CIGSe absorber near the interface will be Cu-depleted. All of these chemical "modifications" are expected to have a significant impact on the electronic structure at the interface and thus on the overall solar cell performance.

The ALS is supported by the Department of Energy, Basic Energy Sciences, Contract No. DE-AC02-05CH11231.

[1] I. Repins, M. A. Contreras, B. Egaas, C. DeHart, J. Scharf, C. L. Perkins, B. To, and R. Noufi, Prog. Photovoltaics **16**, 235 (2008).
[2] N. Barreau, J. C. Bernede, S. Marsillac, C. Amory, and W. N. Shafarman, Thin Solid Films **431–432**, 326 (2003).
[3] D. Hariskos, R. Menner, S. Spiering, A. Eicke, M. Powalla, K. Ellmer, M. Oertel, and B. Dimmler, Proceedings of the 19th European Photovoltaic Solar Energy Conference, Paris, France, 7–11 June 2004.
[4] E. B. Yousfi, B. Weinberger, F. Donsanti, P. Cowache, and D. Lincot, Thin Solid Films **387**, 29 (2001); N. Naghavi, S. Spiering, M. Powalla, B. Canava, and D. Lincot, Prog. Photovoltaics **11**, 437 (2003).
[5] N. A. Allsop, A. Schönmann, H.-J. Muffler, M. Bär, M. C. Lux-Steiner, and Ch.-H. Fischer, Prog. Photovoltaics **13**, 607 (2005).
[6] S. Spiering, A. Eicke, D. Hariskos, M. Powalla, N. Naghavi, and D. Lincot, Thin Solid Films **451–452**, 562 (2004); S. Gall, N. Barreau, S. Harel, J. C. Bernéde, and J. Kessler, *ibid.* **480–481**, 138 (2005).
[7] D. Abou-Ras, G. Kostorz, A. Strom, H.-W. Schock, and A. N. Tiwari, J. Appl. Phys. **98**, 123512 (2005), and references therein.
[8] M. Bär, N. Allsop, I. Lauermann, and Ch.-H. Fischer, Appl. Phys. Lett. **90**, 132118 (2007).
[9] P. Pistor, N. Allsop, W. Braun, R. Caballero, C. Camus, Ch.-H. Fischer, M. Gorgoi, A. Grimm, B. Johnson, T. Kropp, I. Lauermann, S. Lehmann, H. Mönig, S. Schorr, A. Weber, and R. Klenk, Phys. Status Solidi A **206**, 1059 (2009).
[10] N. Barreau, S. Marsillac, and J. C. Bernéde, Vacuum **56**, 101 (2000).
[11] J Klaer, J Bruns, R Henninger, K Siemer, R Klenk, K Ellmer, and D. Bräunig, Semicond. Sci. Technol. **13**, 1456 (1998), and references therein.
[12] C. D. Wagner, W. M. Riggs, L. E. Davis, and J. F. Moulder, in *Handbook of X-Ray Photoelectron Spectroscopy*, edited by G. E. Moulder (Perkin-Elmer, Eden Prairie, 1979), p. 15.
[13] C. Heske, R. Fink, E. Umbach, W. Riedl, and F. Karg, Appl. Phys. Lett. **68**, 3431 (1996).
[14] S. Tanuma, C. J. Powell, and D. R. Penn, Surf. Interface Anal. **21**, 165 (1994); QUASES-IMFP-TPP2M code for the calculation of the inelastic electron mean free path, Version 2.2, http://www.quases.com/.
[15] S. Raud and M.-A. Nicolet, Thin Solid Films **201**, 361 (1991).
[16] R. Hunger, T. Schulmeyer, A. Klein, W. Jaegermann, K. Sakurai, A. Yamada, P. Fons, K. Matsubara, and S. Niki, Surf. Sci. **557**, 263 (2004).
[17] T. Nakada, H. Ohbo, T. Watanabe, H. Nakazawa, M. Matsui, and A. Kunioka, Sol. Energy Mater. Sol. Cells **49**, 285 (1997).
[18] C. Heske, D. Eich, R. Fink, E. Umbach, T. van Buuren, C. Bostedt, L. J. Terminello, S. Kakar, M. M. Grush, T. A. Callcott, F. J. Himpsel, D. L. Ederer, R. C. C. Perera, W. Riedl, and F. Karg, Appl. Phys. Lett. **74**, 1451 (1999); L. Weinhardt, M. Bär, S. Pookpanratana, M. Morkel, T. P. Niesen, F. Karg, K. Ramanathan, M. A. Contreras, R. Noufi, E. Umbach, and C. Heske, Appl. Phys. Lett. (to be published).
[19] J. H. Scofield, J. Electron Spectrosc. Relat. Phenom. **8**, 129 (1976).
[20] For a detailed discussion of the S $L_{2,3}$ spectrum see, e.g., J. Reichardt, M. Bär, A. Grimm, I. Kötschau, I. Lauermann, S. Sokoll, M. C. Lux-Steiner, Ch.-H. Fischer, C. Heske, L. Weinhardt, O. Fuchs, Ch. Jung, W. Gudat, T. P. Niesen, and F. Karg, Appl. Phys. Lett. **86**, 172102 (2005).
[21] N. Barreau and M. Tessier, *Thin-Film Compound Semiconductor Photovoltaics*, MRS Symposia Proceedings No. 1165 (Materials Research Society, Pittsburgh, 2009), p. M08–21.
[22] Calculated using attenuation lengths from B. L. Henke, E. M. Gullikson, and J. C. Davis, At. Data Nucl. Data Tables **54**, 181 (1993); http://www-cxro.lbl.gov/optical_constants/atten2.html.